Appl Phys B (2008) 93: 433–442
DOI 10.1007/s00340-008-3187-z

Applied Physics B
Lasers and Optics

Ionization phase-match gating for wavelength-tunable isolated attosecond pulse generation

A. Jullien · T. Pfeifer · M.J. Abel · P.M. Nagel · M.J. Bell · D.M. Neumark · S.R. Leone

Received: 19 March 2008 / Revised version: 3 June 2008 / Published online: 10 September 2008
© Springer-Verlag 2008

Abstract High-order harmonic emission can be confined to the leading edge of an 800 nm driver laser pulse under moderately intense focusing conditions (7×10^{14} W/cm^2) (Pfeifer et al. in Opt. Express 15:17120, 2007). Here, the experimentally observed curtailment of harmonic production on the leading edge of the driver pulse is shown to be controlled by an ionization-induced phase-matching condition. The transient plasma density inherent to the process of high-harmonic generation terminates the harmonic emission by an ultrafast loss of phase matching on the leading edge of the laser pulse. The analysis is supported by a reconstruction of the in situ intensity envelope of the driver pulse with attosecond temporal resolution, performed by measurements of the carrier-envelope phase dependence of individual half-cycle harmonic cutoffs. The method opens the way to wavelength-tunable isolated attosecond pulse generation.

PACS 42.65.Ky · 41.50.+h · 42.50.Hz · 42.65.Re

A. Jullien (✉) · T. Pfeifer · M.J. Abel · P.M. Nagel · M.J. Bell · D.M. Neumark · S.R. Leone
Departments of Chemistry and Physics, University of California, Berkeley, CA 94720, USA
e-mail: Aurelie.Jullien@ensta.fr
Fax: +33-1-69319996

A. Jullien · T. Pfeifer · M.J. Abel · P.M. Nagel · M.J. Bell · D.M. Neumark · S.R. Leone
Chemical Sciences Division, Lawrence Berkeley National Laboratory, Berkeley, CA 94720, USA

Present address:
A. Jullien
Laboratoire d'Optique Appliquée, ENSTA ParisTech, Ecole Polytechnique, CNRS, UMR 7639, 91761 Palaiseau Cedex, France

1 Introduction

In extreme nonlinear optics, the interaction of a strong laser field with atoms or molecules provides a convenient coherent soft-X-ray source through the generation of high-order harmonics of the incident laser pulse (high-order harmonic generation [HHG]). This highly nonlinear process is well understood through a three-step quasiclassical model [2]. An electron wavepacket first tunnels out of the atomic potential, is accelerated in the laser field and is then finally driven back to the ion. In the last step, recombination to the ground state leads to the emission of an ultrashort coherent burst of light. The characteristics of the emitted radiation depend on the properties of the recolliding electron wave packet. The entire process is repeated every half optical cycle of the driver pulse and gives a harmonic comb in the spectral domain whose energy extends up to the so-called cutoff energy. One of the most attractive characteristics of these soft-X-ray sources is the ability to produce light pulses with durations of a few hundred attoseconds. It has been demonstrated that one can generate either a train of attosecond pulses in the temporal domain [3, 4] or, using a few-cycle driver pulse, isolated attosecond pulses synchronized with the driving laser field [5, 6], opening the way to atomic and molecular spectroscopy with unprecedented temporal resolution [7, 8]. In the regime of few-cycle driver pulses, the stabilization and determination of the carrier-envelope phase (CEP, commonly defined as the offset between the maximum of the electric field and the peak of the pulse envelope) of these ultrashort pulses are required. Indeed, the production of isolated attosecond pulses is typically enabled if the shortest-wavelength harmonic radiation is temporally confined to one half-cycle and thus emitted only once per pulse. So far, this condition has been achieved by intensity discrimination between successive half-cycles in ultrashort

pulses with a CEP fixed to 0 (cosine waveform) [5, 9], by a polarization gating technique [6, 10], or multicolor driving pulses [11–14].

Furthermore, in the few-cycle regime, the extreme sensitivity of the HHG process to the strength of the electric field for each half-cycle and to its position within the pulse envelope provides access to new measurements of various characteristics of the electric field. In particular, individual observable half-cycle cutoffs (HCOs) have been theoretically predicted [15], recently experimentally demonstrated and used to retrieve the absolute value of the CEP of the driver laser pulse [16].

Previously, we have used the characterization method provided by HCO measurements as a function of CEP to demonstrate the confinement of harmonic emission to the leading edge of the driver pulse, attributed to some form of an ionization gating mechanism [1]. The consequence of this particular regime is the ability to restrict the harmonic emission to only one or two half-cycles on the leading edge of the driver pulse, enabling the production of isolated attosecond pulses.

In this paper, we present detailed measurements and calculations aimed at a deeper understanding of the leading-edge gating mechanism in these experiments. With suitable calculations we show that this mechanism is due to ionization-induced phase mismatching between the fundamental and harmonic beams and that the method can be used to control the production of wavelength-tunable isolated attosecond pulses. The results are compared to previous studies of laser-induced ionization gating techniques that rely either on microscopic [17, 18] or macroscopic [19] effects. The analysis is supported by the attosecond time-resolved reconstruction of the experimental time-dependent intensity of the driver pulse during the interaction, based on HCO CEP dependence measurements.

2 Reconstruction of the temporal intensity and instantaneous phase of driver pulses with sub-cycle resolution

When the electric field of the HHG driver pulse is composed of several half-cycles whose extrema vary significantly from one to another (i.e., when there is a large change in the pulse envelope intensity over one optical cycle) specific features appear in the harmonic spectra. In particular, it is already established that the specific cutoff of the harmonic emission of each individual half-cycle is detectable in the overall harmonic spectrum [16]. These half-cycle cutoffs (HCOs) are visible as spectral local maxima: HCO photon energies are determined by measuring the positions of successive maxima of the slow modulation in the high-harmonic spectrum. HCOs are thus easily localized by filtering out the harmonic modulating component (at $2\omega_{\text{laser}}$) by Fourier analysis [1]. The energies of successive HCOs in a given harmonic spectrum strongly depend on the electric field strength extremum of the corresponding half-cycles, and therefore the HCO values carry information about the pulse intensity envelope and CEP. In this section, we explain the principle of the temporal intensity reconstruction of the harmonic-generating portion of the driver pulse with sub-cycle temporal resolution, enabled by the observation of HCO energies as a function of CEP. We demonstrate that the analysis can give access to the electric field characteristics (amplitude and phase). For illustration purposes, we discuss the general methodology using a Gaussian-shaped driver pulse.

The evolving energies of the HCOs with CEP can be predicted by a classical model [2, 20]. For this calculation, the full transient electric field on the leading and trailing edges of a short (sub-10 fs) Gaussian pulse is taken into account. For each half-cycle, the HCO is determined by the maximum kinetic energy accumulated by the returning electron. The model calculates the HCO energy of one half-optical cycle for a given CEP value. When the CEP is changing, the half-cycle is moving relative to the pulse envelope and the corresponding HCO energy can be plotted as a function of CEP. In a general way, because several half-optical cycles of the laser electric field are interacting simultaneously, this dependence is repeated with a shift of π radians (1/2 optical cycle). This is illustrated in Fig. 1a where HCO energies of an 8 fs Gaussian driver pulse are plotted as a function of CEP and optical cycle (gray lines). The Gaussian temporal dependence of the intensity envelope, or more precisely the ponderomotive potential envelope, of the pulse employed for the calculation is also represented (red line). The envelope shape is perfectly superimposed on the calculated lines for the HCO-energy dependence on CEP. Therefore, the HCO energies can be estimated by the following simple formula, an extension of the well-known cut-off law: $E_{\text{HCO}} = I_p + 3.17U_p$ (where U_p is the time-dependent ponderomotive potential of the laser field linked to the electric field extremum and I_p is the ionization potential of the target gas).

Scanning successive HCO energies as a function of CEP is equivalent to directly scanning the experimental ponderomotive potential envelope and allows the reconstruction of the ponderomotive potential time dependence on an optical-cycle time scale. This method provides an in situ characterization of the HHG driver pulse. Indeed, knowing the laser frequency will allow the time-dependent experimental intensity to be deduced from the ponderomotive potential value. As will be shown in the experimental sections, a picture of the evolution of the ponderomotive potential, or equivalently the laser intensity, on a sub-cycle time-scale (resolution limited by CEP increment and stability) during the interaction with the harmonic gas is then accessible, providing a tool to

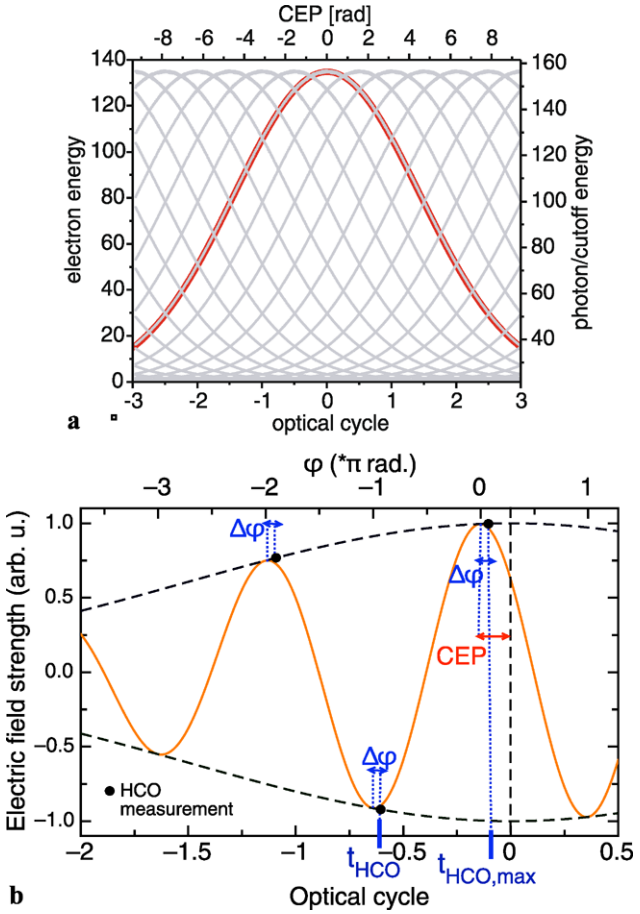

Fig. 1 (**a**) HCO energies as a function of CEP (*gray lines*) calculated with a classical model (see text) for an 8 fs driver pulse. The HCO lines perfectly match the corresponding Gaussian laser pulse intensity envelope (8 fs full width at half maximum (FWHM)). (**b**) To illustrate that HCO measurements can enable the reconstruction of the electric field of the driving pulse, the Gaussian envelope (*black dashed line*) and the electric field (*orange line*) of a 2.5-cycle FWHM pulse with an arbitrary CEP value are plotted on this graph. $\Delta\varphi = 0.26$ rad is the phase between the electric field extremum of the half-cycle and the effective electric field strength whose squared value gives the ponderomotive potential linked to the HCO (*black points*). As a consequence, the electric field (amplitude and phase) can be deduced on an optical cycle time scale by a simple measurement of the HCO energy for an arbitrary and unknown CEP value. The knowledge of the instantaneous frequency allows to convert the optical cycle scale to a femtosecond scale and gives access to the complete reconstruction of the electric field. Each HCO energy ($I_p + 3.17U_p$, with U_p related to the electric field strength of the black points) also provides the temporal evolution of the ponderomotive potential and intensity of the driver pulse

study the influence of various experimental parameters on the infrared pulse and consequently on the HHG process.

Moreover, information related to the electric field and not only to the pulse envelope can be extracted. It is well known that the CEP (φ_0), or absolute phase, is the phase of the electric field for $t = 0$ ($\varphi_0 = \varphi(t = 0)$), where $t = 0$ corresponds to the peak of the pulse envelope. However, for some applications, it can be necessary to have access to the phase of the electric field on the rising edge of the pulse, if the process under study occurs mainly on the rise and not at the peak. In particular, for a given harmonic spectrum, HCO positions can give access to the instantaneous phase $\varphi(t)$. If t_{HCO} is the time at which the emission of one particular HCO occurs, the classical model enables the related instantaneous phase ($\varphi(t = t_{\mathrm{HCO}})$) of the electric field to be calculated. To do so, we note that there is a phase offset ($\Delta\varphi$) between the electric field extremum and the envelope point whose ponderomotive potential value corresponds to an HCO, as illustrated in Fig. 1b. The origin of $\Delta\varphi \neq 0$ relies on the fact that the highest kinetic energy of the returning electron (HCO) is not proportional to an instantaneous field strength but is related to the field evolution between time of ionization and recombination. In the specific case of an 8 fs driver pulse, the classical model estimates $\Delta\varphi$ to be 0.26 rad. This value is close to the one obtained by quantum mechanical calculation for a 5 fs pulse in reference [15] (0.35 rad) and depends only slightly on the pulse duration. We emphasize that the fact that this value (0.26 rad $\approx 15°$) is close to the ionization time resulting in the highest kinetic energy upon recombination ($\omega t = 17°$ [2]) is just a coincidence as it has a different physical origin.

Figure 1b summarizes these notions and illustrates that, as a consequence, the electric field can be deduced on an optical-cycle time scale from the HCO energies. The phase of the electric field is defined relatively to $\varphi(t = t_{\mathrm{HCO,max}})$, with $t_{\mathrm{HCO,max}}$ being the time the most energetic detected HCO is visible. Measurement (or assumption) of the conventionally defined CEP value with respect to the peak of the pulse envelope and an accurate value of the pulse duration are not necessary. Furthermore, a precise knowledge of the instantaneous frequency of the field, which could for instance be extracted from the spacing of the harmonics in the cutoff region for various CEP values, would allow a complete reconstruction of the electric field on a femtosecond time scale. The method is valid assuming that the driving electric field is not distorted on a sub-cycle timescale. The experimental reconstruction of the electric field following HHG in neon with sub-10 fs pulses as performed in reference [21] did not indicate such strong distortion.

In the next sections, HCO analysis is performed on experimental HHG spectra. A non-leading-edge-gated regime is presented first, which illustrates the proposed concepts, followed by leading-edge gating results.

3 High-harmonic generation without leading-edge gating

Experiments are performed with a commercial Ti:sapphire femtosecond laser (Femtolasers Compact Pro) delivering 800 μJ, 25 fs pulses at 3 kHz repetition rate. A hollow-core fiber filled with neon (1.7 bar) and a chirped-mirror

compressor provide external pulse compression to the few-cycle regime (about 6 fs according to second-order interferometric autocorrelation) [22]. A pair of glass wedges allow fine adjustment of the pulse dispersion. Laser pulses are CEP stabilized with a root-mean-square stability of about 200 mrad [23, 24]. The driver pulse is focused by a 400-mm-focal-length mirror, reaching an intensity in the focus, estimated by means of Gaussian beam propagation, of approximately 4×10^{15} W/cm^2. For high-order harmonic generation, a 2-mm-long gas cell with ∼100 µm diameter holes on each side filled with neon is employed. The measured backing pressure (measured in the gas supply line) is 150 mbar. The pressure is optimized for maximum conversion efficiency for the particular cell position, which is placed after the focus to reduce the intensity in the interaction region and select short electron trajectories [25, 26]. Two Zr filters (0.2 µm thickness each) then remove the near-infrared light and low-order harmonics. The remaining radiation is sent to a soft-X-ray spectrometer composed of a transmission grating (on a Si_3N_4 substrate) and a soft-X-ray sensitive CCD.

Two characteristic soft-X-ray spectra measured for different relative CEP values are shown in Fig. 2. To observe the Al absorption L-edge, the high-harmonic spectrum is also measured with two 0.3 µm Al foils instead of Zr (dashed gray line). The positions of the silicon (grating material) and aluminum edges are then used for spectral calibration, allowing us to extract from the harmonic spacing the value of ω_{laser} which is estimated to be 1.7 eV (730 nm). This value agrees with the center wavelength of the driver pulse after spectral broadening in the hollow fiber. The harmonic spectra are very similar to previously published results acquired with similar experimental setups [27]. One spectrum (CEP value labeled φ_0) exhibits a clear continuum in the cutoff region. This continuum is centered at 96 eV, with a bandwidth of 6 eV. This part of the spectrum could be spectrally filtered out in order to isolate an attosecond burst, which is not done here. In contrast, in this same spectral range, individual harmonics are resolved for a CEP value of $\varphi_0 + \pi/2$, in agreement with former observations [28].

Local maxima in the spectrum envelope, observed at different photon energies depending on the CEP value, indicate the individual HCO positions [16]. To further investigate the interaction, HCO analysis has been performed by measuring harmonic spectra for a relative CEP varying from 0 to 3π in $\pi/10$ steps. The CEP-dependence of the HCO energy was then extracted by filtering out the harmonic modulation (at $2\omega_{\text{laser}}$) by means of Fourier analysis. Resulting spectra and HCO positions are plotted in Fig. 3a. HCO positions extracted from this figure are fitted with good agreement by the theoretical HCO energies calculated with a Gaussian laser pulse of 6 fs in Fig. 3b. As shown in Sect. 2, the measured HCO energies are proportional to the ponderomotive potential of the pulse. Unfolding the CEP values using the π-periodicity provides the related experimental ponderomotive potential reconstruction on an optical-cycle timescale (Fig. 3c). For simplicity, we then assume in this study that the instantaneous frequency is constant over the explored time range. A time-dependent intensity reconstruction of the rising edge of the pulse can thus be deduced from the ponderomotive potential dependence (Fig. 3c). Furthermore, HCO energies are linked to the electric field strength extremum and the reconstruction of a part of the electric field envelope is shown in Fig. 3d. In the same figure, the electric field generating the most energetic HCO at $t = t_{\text{HCO,max}}$ is represented. This is enabled by the calculation of $\varphi(t = t_{\text{HCO,max}})$, as explained in Sect. 2. In this experimental regime, $t_{\text{HCO,max}}$ coincides with the peak of the pulse envelope.

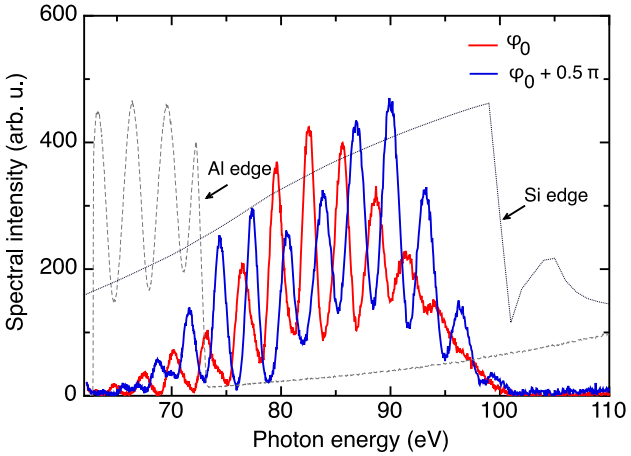

Fig. 2 High-harmonic spectra obtained with Zr filters (*solid lines*) for different CEP values. The transmission of the Si_3N_4 grating material is shown by the *dotted black line*. The spectrum recorded with Al filters (*dashed gray line*) enables the spectral calibration with the Al absorption L-edge

In all graphs of Fig. 3, the data are fitted by a Gaussian 6 fs pulse (FWHM). The choice of a Gaussian shape for the overall pulse is arbitrary and the fit is only intended as a guide to the eye, because the measurement does not give access to the global pulse shape. However, the interacting portion of pulse that produces the harmonics is experimentally accessible and precisely temporally reconstructed, allowing one to assess, in this regime, that the rising edge of the pulse up to the maximum intensity of the envelope is interacting and contributing to the harmonic emission. The energy of the measured HCOs provides a picture of the in situ intensity profile, without the need for pulse duration or beam size measurements. Assuming a constant frequency, the precision on the peak intensity measurement ($(4.3 \pm 0.1) \times 10^{14}$ W/cm^2) is limited by the CEP instability and the error bars when reading the HCO positions. The truncation of the HHG process on the trailing edge is due to a sudden decrease in the efficiency of the HHG process

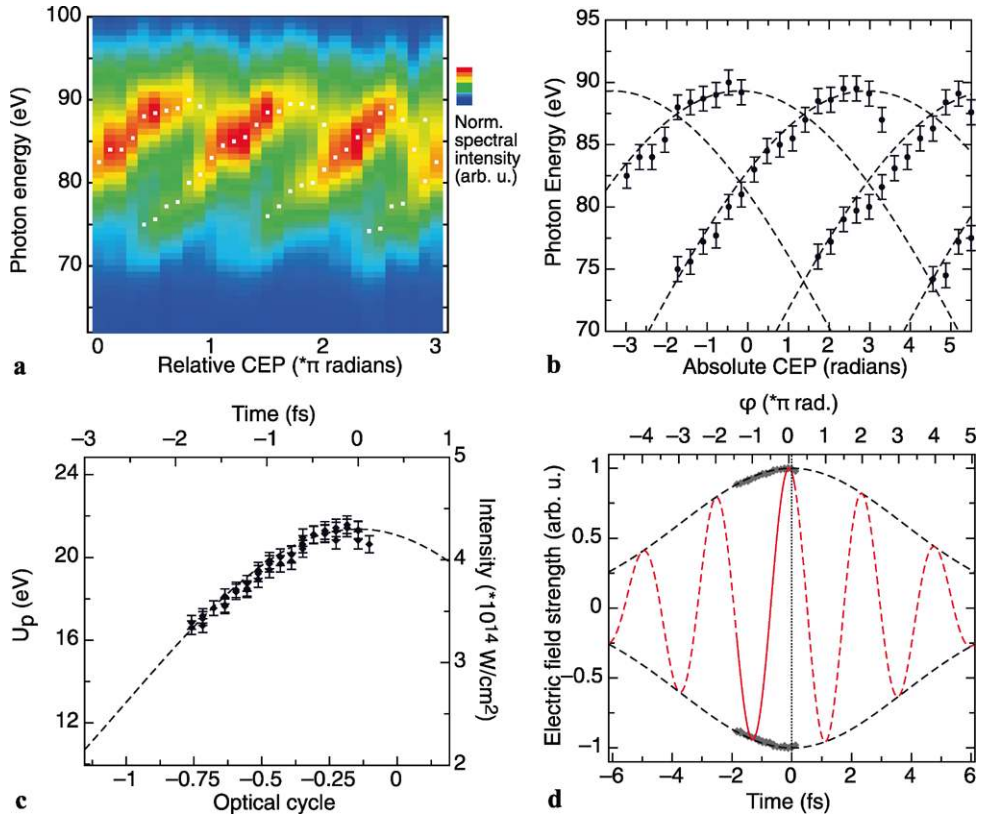

Fig. 3 HHG without leading-edge gating. (**a**) Harmonic spectra as a function of the relative CEP. The harmonic modulation is removed by a mathematical Fourier filtering. The HCO positions (local maxima) for each spectrum are marked with white points. The backing gas pressure is 150 mbar. (**b**) Experimentally recorded HCO energies as a function of CEP (*black points*, extracted from (**a**)) are fitted by theoretical HCO energies calculated with a Gaussian driver pulse of 6 fs, with a peak intensity of 4.3×10^{14} W/cm^2. In this regime the most energetic HCO is emitted at the maximum pulse intensity. (**c**) Unfolding the HCO data from (**a**) leads to the reconstruction of the ponderomotive potential of the laser pulse during the experiment. Assuming a constant frequency, the time-dependent intensity of the harmonic generating part of the pulse can be deduced from the ponderomotive potential and reconstructed with attosecond time resolution. (**d**) HCO measurements give access to a part of the electric field envelope. The represented electric field (*red solid line* for the experimentally accessible temporal window) that generates the most energetic detected HCO (visible at $t = t_{\mathrm{HCO,max}}$, *dotted line*). $\varphi(t = t_{\mathrm{HCO,max}})$ can be calculated and the phase of the electric field is displayed relatively to this value. In this particular regime, $t_{\mathrm{HCO,max}} = 0$, and $\varphi(t = t_{\mathrm{HCO,max}})$ is the CEP

caused by ionization of the target gas [1]. The ability to reconstruct the temporal characteristics of the driver pulse is used in the next section to investigate the mechanism of the sub-cycle ionization gating process.

4 Phase-match gating on the leading edge of the driving pulse

The regime where the high-harmonic emission is gated on the leading edge of the driver pulse is reached by increasing the laser intensity in the interaction region. This is experimentally realized by moving the cell towards the focus of the driver pulse. The peak intensity in this case cannot be experimentally determined, as explained below, but it will become clear that the exact value of the driver pulse peak intensity is no longer of prime importance for isolated attosecond pulse generation in the gated regime.

Figure 4 shows typical spectra obtained for different CEP values and a backing pressure of 200 mbar. We observed that the on-axis brightness of the harmonic beam is higher than in the non-gated regime. The generated radiation extends up to 115 eV and exhibits, for specific CEP values with a π-periodicity, a continuous feature with a bandwidth of approximately 10 eV. The overall minimum transmission occurring beyond 100 eV corresponds to the absorption edge of Si in the spectrometer grating material. To remove this transmission artifact for the HCO energy measurements, the harmonic spectra plotted in Fig. 5a as a function of the phase are normalized by dividing by the CEP average after removal of the $2\omega_{\mathrm{laser}}$ modulation. The CEP dependence of the HCO energies is dramatically different from the one observed in Sect. 3. The HCO energies evolve linearly with the CEP following a constant slope and do not exhibit the saturation expected when the most energetic part of the spectrum is generated near the peak of the pulse. In Fig. 5b,

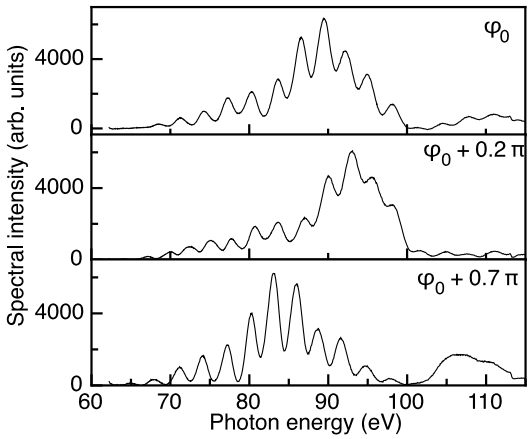

Fig. 4 High-harmonic spectra measured in the gated regime for various CEP values. A continuum is observable for some CEP values. The gas pressure is 200 mbar

the HCO positions are fitted by the leading edge of a 7 fs, 6.7×10^{14} W/cm^2 pulse with a good agreement. The reconstructed temporal dependence of the experimental ponderomotive potential is shown in Fig. 5c. In Fig. 5d, the electric field envelope deduced from Figs. 5a and 5b and the electric field generating the most energetic HCO are represented. It becomes clear that in this particular regime, when the process mainly occurs on the leading edge, $\varphi(t = t_{\mathrm{HCO,max}})$ is more appropriate to characterize the phase of the electric field than the knowledge of the CEP, which is meaningless in this specific case.

The gating of the harmonic emission on the leading edge clearly appears in the temporal intensity reconstruction of the interacting part of the pulse (Figs. 5c and 5d). The harmonic radiation is curtailed at some point on the rising edge of the pulse, at a laser intensity of $(5.6\pm0.1)\times10^{14}$ W/cm^2. The generation of continuous spectra is an indication that no harmonic light is emitted after the closure of the gate and that we do not "miss" another HCO. Closure of the gate is measured with a precision dependent on the experimental CEP increment ($\pi/10$), to better than 300 as. Some fits of the experimental data with different pulse durations and peak intensities also provide convincing results. As was pointed out, neither the infrared pulse duration, maximum laser intensity, or CEP as conventionally defined are accessible in this leading-edge-gated regime [1]. However, because the maximum of the pulse envelope is not generating harmonic light, the knowledge of these values is not of prime importance. In the gated regime the pertinent quantity is the slope of the rising edge of the ponderomotive potential (or intensity) envelope which is experimentally accessible. This value is related to the difference in intensity between successive half-cycles and consequently to the maximum width of the HHG continuum that can be generated. Gating the harmonic emission on the leading edge of the driver pulse therefore significantly increases the available continuum bandwidth. This is demonstrated here by a comparison between the results obtained in this section and those shown in Sect. 3. In the leading-edge-gated regime, the continuous region of the harmonic spectrum is 50% broader than in the non-leading-edge-gated case (10 eV compared to 6 eV), without the need for further driver pulse shortening or additional schemes such as a polarization gate.

We now consider the mechanism for gate closure in more detail. Some microscopic laser-induced ionization effects that rely on complete depletion of the ground state, which could create this ionization gate, have already been reported [18, 29]. More recently, Cao et al. have proposed a theoretical high intensity pulse scheme (21 fs, 2.5×10^{15} W/cm^2) to deplete the ground state completely on the leading edge of the pulse, enabling single attosecond pulse generation in the multicycle regime [17]. To calculate the ionization rate and extent of ionization in our experimental regime, we used two different models: the well-accepted ADK (Amnesov, Delone, and Krainov) formula in the tunnelling regime [30] and a CEP-dependent analytical model demonstrated for various values of the Keldysh parameter (γ, $\gamma^2 = \frac{I_p}{2U_p}$) [31]. For the laser intensity employed (above 10^{14} W/cm^2, in neon $\gamma < 1$), the two models provide consistent results. Experimentally determined absolute intensity values from Fig. 5c indicate that at the closure of the gate, only $\simeq$1.5% of the medium is ionized. Variation of this value with the laser CEP is negligible. Consequently, the single-atom response cannot satisfactorily explain the experimental behavior: closure of the gate does not coincide with the complete depletion of the ground state.

However, the degree of ionization of the target gas has a crucial influence on the phase mismatch between the fundamental infrared and harmonic beams that results from different phase velocities. This phase mismatch is one of the main limitations for HHG conversion efficiency. Related issues have often been discussed [26, 32–34] and several solutions have been proposed to control and enhance phase-matching conditions [35–38]. For instance, a scheme of time-gated phase matching by pulse shaping in a hollow waveguide allows the creation of a short phase-matched window between the leading edge and trailing edge of the pulse, enabling efficient selection and enhancement of one given harmonic [19].

Furthermore, reference [34] estimates that, without any specific geometrical configuration to improve phase matching, the critical extent of ionization for neon is 1.1%: once the fraction of free electrons becomes higher, perfect phase matching is no longer possible and the conversion efficiency starts to drop. To estimate the influence of these macroscopic factors, we performed a simple calculation of phase matching including the plasma-induced dispersion linked to the free-electron density, the linear dispersion in neon between the harmonic light and the infrared pulse, and a prop-

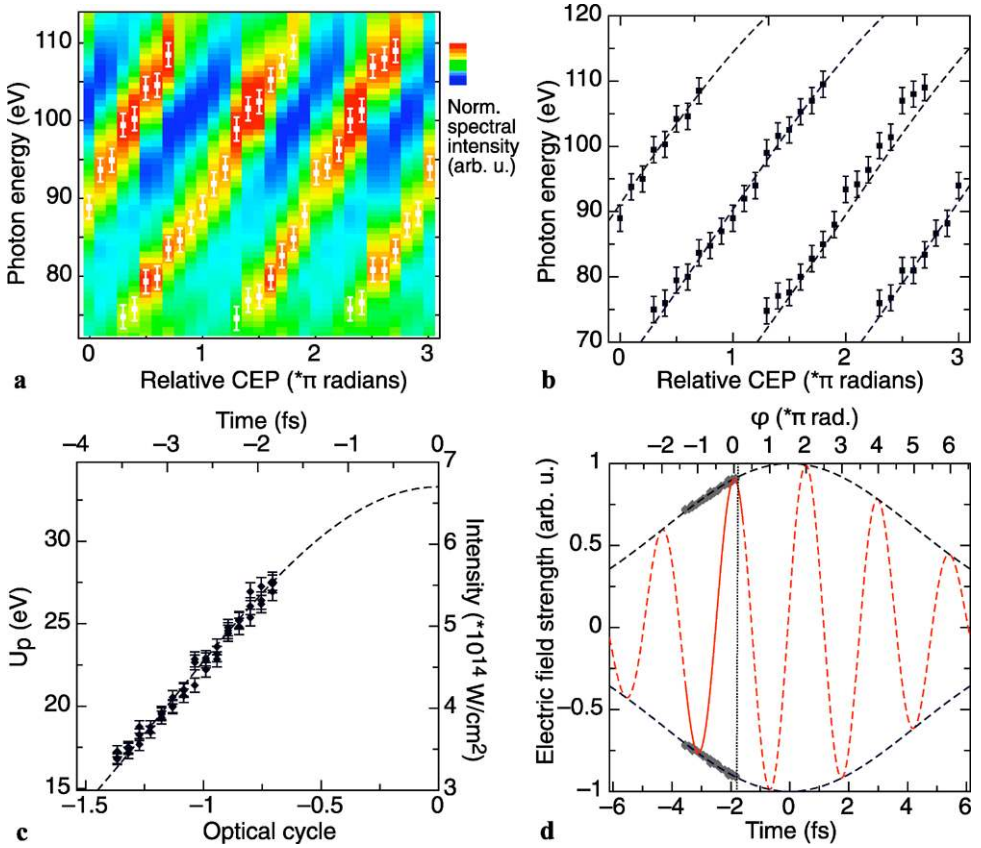

Fig. 5 HHG in the leading-edge gating regime. (**a**) Harmonic spectra as a function of the relative CEP. The harmonic modulation is removed by a mathematical Fourier filtering. The HCO positions (local maxima) for each spectrum are marked with *white points*. The backing gas pressure is 200 mbar. (**b**) Experimentally recorded HCO energies as a function of CEP (*black points*, extracted from (**a**)) are fitted by theoretical HCO energies calculated with a Gaussian driver pulse of 7 fs, with a peak intensity of 6.7×10^{14} W/cm^2. (**c**) Unfolding the HCO data from (**a**) leads to the reconstruction of the ponderomotive potential of the laser during the experiment. Assuming a constant frequency, the time-dependent intensity of the harmonic generating part of the pulse can be deduced from the ponderomotive potential and reconstructed with attosecond time resolution. (**d**) HCO measurements give access to a part of the electric field envelope. The represented electric field (*red solid line* for the experimentally accessible temporal window) that generates the most energetic detected HCO (visible at $t = t_{\mathrm{HCO,max}}$, *dotted line*). $\varphi(t = t_{\mathrm{HCO,max}})$ can be calculated and the phase of the electric field is displayed relatively to this value. $\varphi(t = 0)$ is not accessible in this case. The *red solid line* used for the electric field curve illustrates the limits of the experimentally accessible temporal window

agation term (linked to the Gouy phase shift) considering that the cell is placed in our setup after the Rayleigh distance [34, 39]. Because only the central part of the beam is analyzed, the plane wave approximation is assumed. We assume the interaction length to be 3 mm (the cell length is 2 mm, but the effective interaction length is greater because of gas diffusion along the axis). The measured backing gas pressure is typically around 200 mbar. As the gas pressure in the cell is unknown, we define an effective pressure, which would correspond to the averaged pressure along the interaction length and is consequently lower than the backing pressure. The high-harmonic generation efficiency is then proportional to the phase matching factor defined as $\mathrm{sinc}^2(\frac{\pi L_{\mathrm{int}}}{2L_{\mathrm{coh}}})$ (L_{int} and L_{coh} being the interaction and coherence lengths, respectively, $L_{\mathrm{coh}} = \frac{\pi}{\Delta k}$ with Δk the phase mismatch between the fundamental and harmonic light waves).

Results of the calculation are shown in Fig. 6 for several experimental configurations. In each case, the cell position with respect to the focus is estimated by Gaussian beam propagation to be consistent with the laser pulse peak intensity used to fit experimental data. For the leading-edge-gated regime (Figs. 6a and 6b), the effective pressure is fixed to 100 mbar, below the measured backing pressure, and mainly affects the phase-matching factor for negative time infinity. Fig. 6a presents the absolute experimental intensity data extracted from HCO measurements (Fig. 5), fitted by a Gaussian pulse with a duration of 7 fs and a peak intensity of 6.7×10^{14} W/cm^2, the corresponding extent of ionization and the calculated phase-matching factor. The transient plasma density truncates the harmonic phase matching on the leading edge of the driver pulse when the extent of ionization is above the percent level, in a quantitatively concordant way with the experimental behavior. We

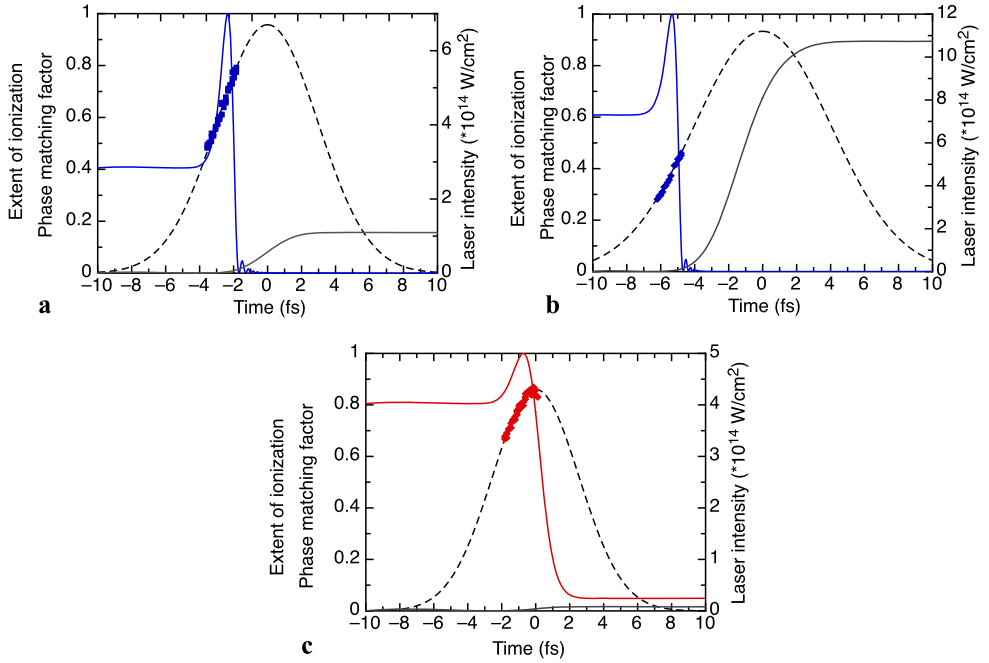

Fig. 6 Illustration of the ionization-gate principle. Calculated phase-matching factor (see text, *left* y-scale) is plotted for a harmonic wavelength of 10 nm and an interaction length of 3 mm (*solid red* and *blue lines*) for various driving laser pulse intensity profiles (*dashed lines*, *right* y-scale). The corresponding extent of ionization of the medium is represented by *gray lines* (*left* y-scale). (**a**) Leading-edge-gated regime. Experimentally reconstructed intensity envelope (*blue squares*) extracted from HCO measurements (Fig. 5) is fitted by a 7 fs, 6.7×10^{14} W/cm^2 Gaussian pulse. (**b**) The same experimental data are fitted by a 10 fs, 1.1×10^{15} W/cm^2 Gaussian pulse. In both cases, the effective pressure in the HHG cell is taken to be equal to 100 mbar and the transient plasma density under the envelope of the driver pulse shuts down the harmonic phase matching on the leading edge. (**c**) When the laser peak intensity decreases, the ionization rate is lower and the loss of phase matching occurs after the peak of the driver pulse. This is illustrated by using the experimental results presented in Sect. 3 (Fig. 3): the experimental data are fitted by a 6 fs, 4.3×10^{14} W/cm^2 Gaussian pulse. An excellent agreement is obtained between the calculations and experimental measurements

underline that the same experimental data can also be fitted by a laser pulse with different characteristics, as shown in Fig. 6b (Gaussian pulse, 10 fs, 1.1×10^{15} W/cm^2). In that case, the final extent of ionization is higher (90%) but the phase-matching factor evolution is still concordant with the experimentally observed shutdown of the harmonic radiation. This observation indicates that the leading-edge-gated regime for harmonic continuum generation can indeed be reached with a longer (multicycle) and more intense pulses, as proposed in reference [1]. To further illustrate the validity of this simple model, the same calculation is performed for the non-leading-edge-gated regime presented in Sect. 3 (Fig. 6c). In this case, the cell is more distant from the focus (laser peak intensity of 4.3×10^{14} W/cm^2) and the effective pressure is slightly lower (80 mbar) as was the backing pressure before the cell. The extent of ionization remains low (1.7% maximum) and the phase-matching gate is closed after the peak of the driver pulse (when the ionization fraction reaches ~1.5%). The critical parameter is consequently identified as the ionized fraction of the medium, varying highly nonlinearly with the laser intensity. By increasing the laser intensity, the gate resulting from ultrafast loss of phase matching is moved towards the leading edge of the pulse. We believe that the previously observed harmonic cutoffs at photon energies lower than expected from the three-step model in the case of long driver pulses (>100 fs) in tight focusing conditions are another manifestation of the herein discussed phase-matching gate [40].

5 Perspective: isolated tunable attosecond pulses

Significant advantages of the ionization gating regime are apparent once one can control the closure of the gate by tuning the necessary parameters (ionization rate dependence on the laser intensity, gas pressure) and the slope of the ponderomotive potential envelope per optical cycle. It is particularly interesting to optimize the laser compression to produce a steeper rising edge with a slightly shorter pulse of ~6 fs. The pressure is 240 mbar. Resulting spectra and HCO positions as a function of CEP appear in Fig. 7. For each phase value, only one broad HCO is visible. Sometimes, no maximum is detected in the spectrum ($\varphi_0 + 3\pi/4$ and $\varphi_0 + 7\pi/8$) as the difference between two successive HCOs is very large. The rising edge of the pulse is sufficiently steep to provide significant change in the ponderomotive potential

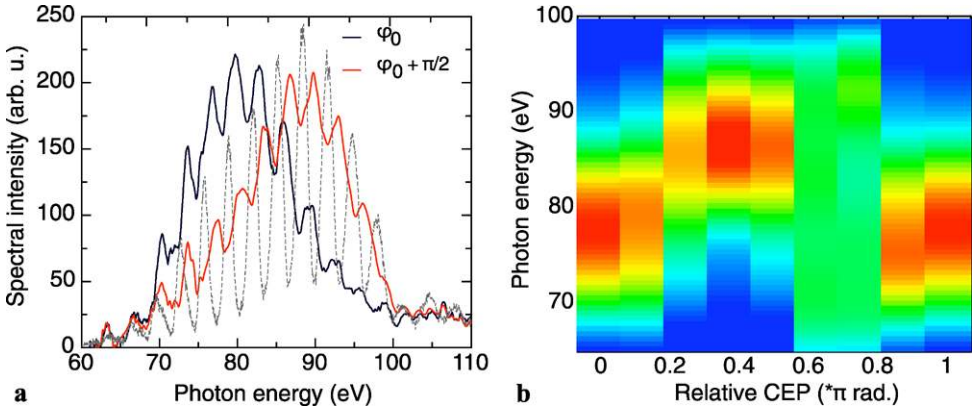

Fig. 7 (**a**) Quasi-continuous high-harmonic spectra (raw data, unfiltered), wavelength-tunable with CEP. A deeply modulated spectrum obtained with a long pulse is shown for comparison (*dashed gray line*).The gas backing pressure is 240 mbar. (**b**) Corresponding harmonic spectra as a function of the relative CEP. The harmonic modulation is removed

from one half-cycle to the next and to isolate the harmonic emission of only one half-cycle before the closure of the gate.

Surprisingly, the gate is closed earlier for this shorter pulse, as the most energetic HCO is emitted around 90 eV. A slightly higher ionization rate due to an ionizing prepulse might be an explanation. Such satellite pulses often accompany ultrashort laser pulses: short pulse generation is known to be a trade-off between pulse duration and coherent temporal contrast.

The resulting spectra (Fig. 7a) exhibit a quasi-continuous shape strongly indicative of an isolated attosecond pulse, regardless of the absolute phase. The remaining weak modulation results from a weaker harmonic burst generated in this energy range by the previous or the next half-cycle. A remarkable feature is the width of the quasi-continuous spectra (15 eV FWHM), enabling the generation of attosecond pulses with a duration of 200 as with an adequate chirp compensation. Shorter pulses have been produced, but require additional polarization gating or state of the art femtosecond pulses (3.5 fs) [6, 9]. Finally, as previously mentioned, the concept of CEP defined at the peak of the pulse envelope becomes meaningless when an ionization gate closes on the leading edge of the pulse. In the ionization gating regime, the phase of the interacting half-cycle becomes a free experimental parameter to tune the central wavelength of the continuous spectral emission.

6 Conclusion

To conclude, HCO analysis can be used for in situ reconstruction of the time-dependent ponderomotive potential and intensity envelope of the laser pulse with attosecond resolution. The analysis can also give access to the complete characterization of the electric field (amplitude and phase). We have used this method to experimentally detect gated harmonic emission on the leading edge of the driver pulse. By choosing various laser intensities, we can switch from the non-gated to the gated regime and we have provided evidence that the gating mechanism relies on the ionization-induced phase mismatching between the fundamental and harmonic fields. This method allows exploitation of the large ponderomotive potential difference between successive half-cycles on the leading edge of the driving pulse. The ionization gating regime enables the generation of broadband quasi-continuous harmonic spectra, tunable with the phase of the half-cycle temporal window that generates harmonics before the ionization gate closure. Finally, the ionization gating mechanism can be extended to multicycle laser pulses as long as the intensity is high enough to guarantee a steep rising edge. In that case, potential prepulses would also reach relatively high intensity. To keep the extent of ionization in the percent level during the interaction, the pulse must exhibit a very good temporal contrast on the leading edge, which can be achieved by a plasma mirror scheme [41] or nonlinear filtering devices [42].

Acknowledgements The authors would like to thank Lukas Gallman for his essential contribution to the laser and phase-stabilization development and Jun Ye and Jason Jones for providing components of the phase-stabilization electronics. This work is supported by a MURI program from the Air Force Office of Scientific research, contract No. FA9550-04-1-0242. Portions of the laboratory infrastructure are supported by the Director, Office of Science, Office of Basic Energy Sciences, of the US Department of Energy under contract DE-AC02-05CH11231. T.P. acknowledges support of a Feodor-Lynen Fellowship of the Alexander von Humboldt Foundation.

References

1. T. Pfeifer, A. Jullien, M.J. Abel, P.M. Nagel, L. Gallmann, D.M. Neumark, S.R. Leone, Opt. Express **15**, 17120 (2007)
2. P. Corkum, Phys. Rev. Lett. **71**, 1994 (1993)
3. P.M. Paul, E.S. Toma, P. Breger, G. Mullot, F. Auge, P. Balcou, H.G. Muller, P. Agostini, Science **292**, 1689 (2001)
4. Y. Mairesse, A. de Bohan, L.J. Frasinski, H. Merdji, L.C. Dinu, P. Monchicourt, P. Breger, M. Kovacev, R. Taieb, B. Carre, H.G. Muller, P. Agostini, P. Salières, Science **302**, 1540 (2003)
5. R. Kienberger, E. Goulielmakis, M. Uiberacker, A. Baltuška, V. Yakovlev, F. Bammer, A. Scrinzi, T. Westerwalbesloh, U.

Kleineberg, U. Heinzmann, M. Drescher, F. Krausz, Nature **427**, 817 (2004)
6. G. Sansone, E. Benedetti, F. Calegari, C. Vozzi, L. Avaldi, R. Flammini, L. Poletto, P. Villoresi, C. Altucci, R. Velotta, S. Sagira, S.D. Silvestri, M. Nisoli, Science **314**, 443 (2006)
7. M. Drescher, M. Hentschel, R. Kienberger, M. Uiberacker, V. Yakovlev, A. Scrinzi, T. Westerwalbesloh, U. Kleineberg, U. Heinzmann, F. Krausz, Nature **419**, 803 (2002)
8. M. Uiberacker, T. Uphues, M. Schultze, A.J. Verhoef, V. Yakovlev, M.F. Kling, J. Rauschenberger, N.M. Kabachnik, H. Schroder, M. Lezius, K.L. Kompa, H.G. Muller, M.J.J. Vrakking, S. Hendel, U. Kleineberg, U. Heinzmann, M. Drescher, F. Krausz, Nature **446**, 627 (2007)
9. M. Schultze, E. Goulielmakis, M. Uiberacker, M. Hofstetter, J. Kim, D. Kim, F. Krausz, U. Kleineberg, New J. Phys. **9**, 243 (2007)
10. N. Dudovitch, J. Levesque, O. Smirnova, D. Zeidler, D. Comtois, M.Y. Ivanov, D.M. Villeneuve, P.B. Corkum, Phys. Rev. Lett. **97**, 253903 (2006)
11. T. Pfeifer, L. Gallman, M.J. Abel, D.M. Neumark, S.R. Leone, Opt. Lett. **31**, 975 (2006)
12. T. Pfeifer, L. Gallmann, M.J. Abel, P.M. Nagel, D.M. Neumark, S.R. Leone, Phys. Rev. Lett. **97**, 163901 (2006)
13. H. Merdji, T. Auguste, W. Boutu, J.-P. Caumes, B. Carré, T. Pfeifer, A. Jullien, D.M. Neumark, S.R. Leone, Opt. Lett. **32**, 3134 (2007)
14. Y. Oishi, M. Kaku, F. Kannari, K. Midorikawa, Opt. Express **14**, 7230 (2006)
15. V.S. Yakovlev, A. Scrinzi, Phys. Rev. Lett. **91**, 153901 (2003)
16. C.A. Haworth, L.E. Chipperfield, J.S. Robinson, P.L. Knight, J.P. Marangos, J.W.G. Tisch, Nat. Phys. **3**, 52 (2007)
17. W. Cao, P. Lu, P. Lan, X. Wang, G. Yang, Phys. Rev. A **74**, 063821 (2006)
18. T. Sekikawa, A. Kosuge, T. Kanai, S. Watanabe, Nature **432**, 605 (2004)
19. A.S. Sandhu, E. Gagnon, A. Paul, I. Thomann, A. Lytle, T. Keep, M.M. Murnane, H.C. Kapteyn, Phys. Rev. A **74**, 061803(R) (2006)
20. S. Kazamias, P. Balcou, Phys. Rev. A **69**, 063416 (2004)
21. E. Goulielmakis, M. Uiberacker, R. Kienberger, A. Baltuška, V. Yakovlev, A. Scrinzi, T. Westerwalbesloh, U. Kleineberg, U. Heinzmann, M. Drescher, F. Krausz, Science **305**, 1267 (2004)
22. M. Nisoli, S.D. Silvestri, O. Svelto, Appl. Phys. Lett. **68**, 2793 (1996)
23. J. Rauschenberger, T. Fuji, M. Hentschel, A.J. Verhoef, T. Udem, C. Gohle, T. Hansch, F. Krausz, Laser Phys. Lett. **3**, 37 (2006)
24. M. Mehendale, S.A. Mitchell, J.P. Likforman, D.M. Villeneuve, P.B. Corkum, Opt. Lett. **25**, 1672 (2000)
25. P. Antoine, A. L'Huillier, M. Lewenstein, Phys. Rev. Lett. **77**, 1234 (1996)
26. P. Salières, A. L'Huillier, M. Lewenstein, Phys. Rev. Lett. **74**, 3776 (1995)
27. M. Uiberacker, T. Uphues, M. Schultze, A.J. Verhoef, V. Yakovlev, M.F. Kling, J. Rauschenberger, N.M. Kabachnik, H. Schroder, M. Lezius, K.L. Kompa, H.G. Muller, M.J.J. Vrakking, S. Hendel, U. Kleineberg, U. Heinzmann, M. Drescher, F. Krausz, Nature **446**, 627 (2007)
28. A. Baltuška, T. Udem, M. Uiberacker, M. Hentschel, E. Goulielmakis, C. Gohle, R. Holwarth, V.S. Yakovlev, A. Scrinzi, T.W. Hänsch, F. Krausz, Nature **421**, 611 (2003)
29. A. Bouhal, P. Salières, P. Breger, P. Agostini, G. Hamoniaux, A. Mysyrowicz, A. Antonetti, R. Constantinescu, H.G. Muller, Phys. Rev. A **58**, 389 (1998)
30. S. Augst, D.D. Meyerhofer, D. Strickland, S.L. Chint, J. Opt. Soc. Am. B **8**, 858 (1991)
31. G.L. Yudin, M.Y. Ivanov, Phys. Rev. A **64**, 013409 (2001)
32. A. L'Huillier, K. Schafer, K. Kulander, J. Phys. B **24**, 3315 (1991)
33. G. Tempea, T. Brabec, Appl. Phys. B **70**, S197 (2000)
34. A. Paul, E.A. Gibson, X. Zhang, A. Lytle, T. Popmintchev, X. Zhou, M.M. Murnane, I.P. Christov, H.C. Kapteyn, IEEE J. Quantum Electron. **42**, 14 (2006)
35. C.G. Durfee, A.R. Rundquist, S. Backus, C. Herne, M.M. Murnane, H.C. Kapteyn, Phys. Rev. Lett. **83**, 2187 (1999)
36. E.A. Gibson, A. Paul, N. Wagner, R. Tobey, D. Gaudiosi, S. Backus, I.P. Christov, A. Aquila, E.M. Gullikson, D.T. Attwood, M.M. Murnane, H.C. Kapteyn, Science **302**, 95 (2003)
37. O. Cohen, X. Zhang, A.L. Lytle, T. Popmintchev, M.M. Murnane, H.C. Kapteyn, Phys. Rev. Lett. **99**, 053902 (2007)
38. X. Zhang, A.L. Lytle, T. Popmintchev, X. Zhou, H.C. Kapteyn, M.M. Murnane, O. Cohen, Nat. Phys. **3**, 270 (2007)
39. S. Kazamias, D. Douillet, F. Weihe, C. Valentin, A. Rousse, S. Sebban, G. Grillon, F. Auge, D. Hulin, P. Balcou, Phys. Rev. Lett. **90**, 193901 (2003)
40. C.-G. Wahlström, J. Larsson, A. Persson, T. Starczewski, S. Svanberg, P. Salières, P. Balcou, A. L'Huillier, Phys. Rev. A **48**, 4709 (1993)
41. G. Doumy, F. Quere, O. Gobert, M. Perdrix, P. Martin, P. Audebert, J.C. Gauthier, J.-P. Geindre, T. Wittmann, Phys. Rev. E **69**, 026402 (2004)
42. A. Jullien, O. Albert, F. Burgy, G. Hamoniaux, J.-P. Rousseau, J.-P. Chambaret, F. Augé-Rochereau, G. Chériaux, J. Etchepare, N. Minkovski, S.M. Saltiel, Opt. Lett. **30**, 920 (2005)